Analysis and Application of Pattern Prediction Techniques for mm-Wave 5G Active Phased Arrays

Jorge Calatayud Maeso[(1)], Fernando Rodriguez Varela[(2)], Alfonso Tomas Muriel Barrado[(3)],
Pablo Sanchez-Olivares[(1)], Jose Manuel Fernandez Gonzalez,[(1)]
jorge.cmaeso@upm.es
[(1)]Information Processing and Telecommunications Center, ETSI Telecomunicación, Universidad Politécnica de Madrid.
Avda. Complutense, 30, 28040 Madrid, Spain
[(2)]Universidad Rey Juan Carlos de Madrid. Av. del Alcalde de Móstoles, 28933 Móstoles
[(3)]Group of RadioFrequency: Circuits, Antennas and Systems (RFCAS),
Escuela Politécnica Superior, Universidad Autónoma de Madrid, 28049 Madrid, Spain

***Abstract*—This paper examines the non-idealities inherent in commercially available beamformers and explores their implications in the calibration procedures for phased array antennas. The non-ideal nature of the beamformer is meticulously modeled and assessed through extensive S-Parameter measurements to discern its impact on analyzed excitation retrieval methods. The Rotating-element Electric-field Vector (REV) and Control Circuit Encoding (CCE) methods are simulated using a synthetic array with spherical wave expansion driven by output coefficients measured from the beamformer. Simulations are executed to compare the REV method with a Selective-REV variant, designed to enhance coefficient prediction accuracy by leveraging a priori knowledge of phase-shifter amplitude deviations. Additionally, amplitude, phase, and complex CCE encodings are employed to determine the encoding technique that best accommodates beamformer non-idealities. Finally, anechoic chamber measurements assess the pattern prediction capabilities of the calibration methods explored in the simulation.**

I. Introduction

Millimeter-Wave technology is integral to the fifth generation of cellular systems (5G), capitalizing on its expansive bandwidth to promise high data rates [1]. However, mm-Wave signals encounter challenges such as elevated path loss due to their heightened carrier frequencies. Addressing these challenges and ensuring adequate signal-to-noise ratios necessitates high-gain reconfigurable antennas. Active phased arrays with adaptive beamforming are pivotal not only for mitigating propagation degradation but also for dynamically reallocating resources based on demand. Despite the significant power requirements of digital beamforming in these arrays due to their high element count, hybrid and analog beamforming offer compelling solutions by achieving reconfigurability within a lower total power budget [2].

Nevertheless, analog beamformers operating in millimeter wave bands suffer from many non-idealities, such as amplitude variations induced by the selected phase setting or interchannel coupling [3], [4]. Accurate evaluation and diagnosis of these errors in phased array antennas is essential. It is even more relevant when the proposed architecture relies on multiple smaller arrays instead of a single larger array, where apperture errors result more significant. Additional errors induced by the degradation of the RF components over time should also be measureble. Due to the high volume of micrometer wave systems deployed, offline calibration may be economically unfeasible, so establishing on-site diagnosis models and methods may be the only choice to prolong the life cycle of this equipment.

II. Undesired effects on highly integrated beamformers

Planar phased array antennas at mm-wave bands have tight space constraints to place their circuitry [5]. Therefore, it is key to integrate as many components of the RF chain into this small available space as possible. One of the most successful commercial state-of-the-art solutions for a transmit beamformer is based on the integration of eight independently controllable RF front-ends formed by a common VGA amplifier to compensate for signal splitting and amplitude and phase control for each branch based on a 4 to 6 bit phase shifter and attenuator with an independent amplifier [4]. The architecture illustrated in Fig. 1 shows the general diagram for a commercial beamformer from the Xphased brand which has a 6bit phase shifter and 30dB of attenuation control with 0.5dB jumps.

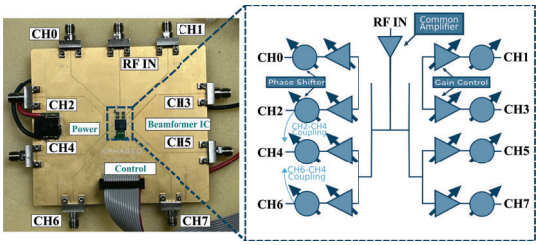

Fig. 1. Beamformer evaluation board and internal signal path diagram

Ideally, the complex output coefficient (V_i) for the i-th channel of the beamformer is represented with Eq. 1, where α_i and β_i are the programmed amplitude and phase bit-states for the i-th channel, ΔA and $\Delta\phi$ are the phased and amplitude control increments.

$$V_i = A_i(\alpha_i)e^{j\Phi_i(\beta_i)} = (\alpha_i \Delta A)e^{j\beta_i \Delta\phi} \quad (1)$$

However, after measuring the beamformer using the setup shown in Fig. 2, the amplitude of the coefficient varies depending on the programmed phase state (Figs. 3(a), 3(b)) due to the phase-shifter loss variance. Nevertheless, the phase jump of the phase shifter, as measured in Figs. 3(c), 3(d), is

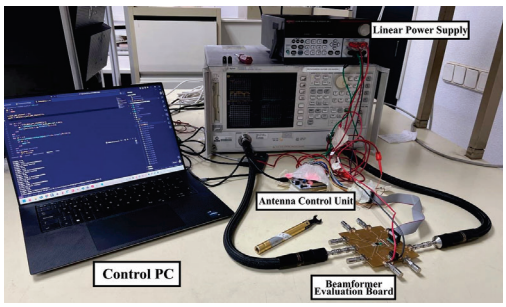

Fig. 2. Test setup for validation of the behavior model of the output coefficients of the commercial beamformer

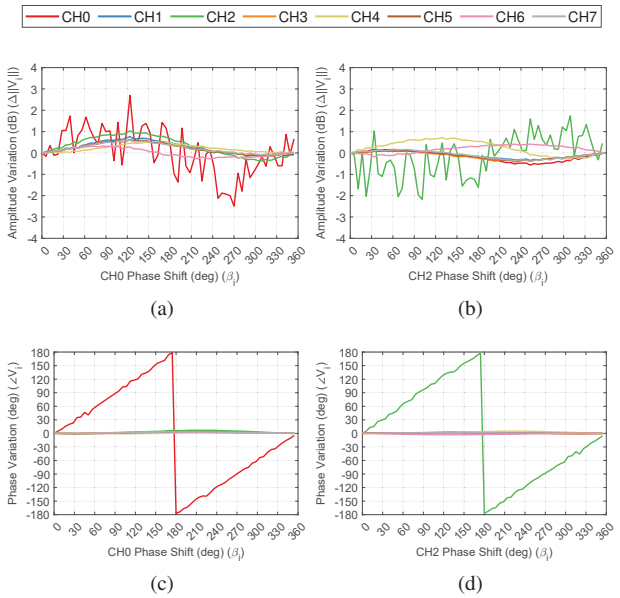

Fig. 3. Amplitude and phase variation induced when the phase shifter of the channel [(a,c) CH0 (b,d) CH2] is swept

considered ideal, leading to $V_i = A_i(\alpha_i, \beta_i)e^{j\beta_i \Delta\phi}$. Furthermore, when the adjacent channel phase is swept the amplitude of the nearby channels also varies. This amplitude variation, with a sine-like shape, is due to internal coupling between channels on the beamformer and represents an additional contribution to the channel output coefficient. To model all the signal contributions to the output coefficient, Eq. 2 is proposed. Eq. 2 adds a coupling term in the form of a sum of the contribution of the interfering channels, whose intensity is modeled by C_n, which depends on the configured amplitude state of the interfering channel. This coupling term can become more significant than the direct term generating an attenuation floor effect as shown in Figs. 4(a), 4(b).

$$V_i = A_i(\alpha_i, \beta_i)e^{j\beta_i \Delta\phi} + \sum_{\substack{n=1 \\ n\neq i}}^{N} C_n(\alpha_n)e^{j\beta_n \Delta\phi} \quad (2)$$

III. Application of Calibration Methods to mm-Wave Beamformers

A. Peripheral probe calibration for active phased arrays

The main limitation to calibrating a millimetre-wave phased array induced by the beamformer is the interaction between each channel configuration. Peripheral probe methods, which

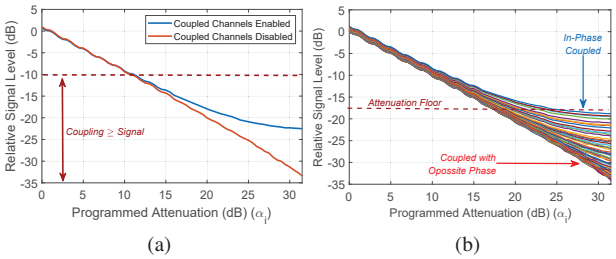

Fig. 4. Signal attenuation measured when (a) coupled channels are turned on/off (b) the channel under measure modify its phase

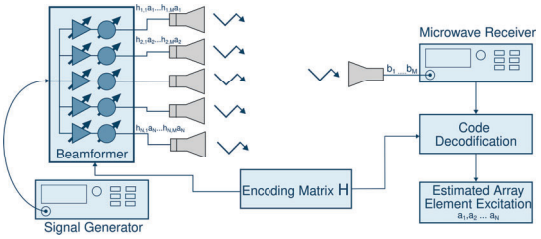

Fig. 5. Setup for peripheral probe calibration methods

are based on some signal encoding, allow the extraction of the excitation coefficient of a given element when the rest of the elements are in their operating condition. Fig. 5 illustrates the usual test setup used by these methods. These kinds of methods allow the calibration of each element taking into consideration the contribution of the interchannel coupling. However, the amplitude variance induced by phase change generates additional errors when decoding the received signals. Two of the most popular peripheral probe methods are the REV method [6] and the Control Circuit Encoding (CCE) techniques [7].

B. The REV Method

The Rotating-element Electric-field Vector (REV) method is an array calibration method based on the superposition of the fields radiated by each element that resembles the array [6]. The total field radiated by an array of N elements in a given configuration ($\vec{E}_{array}$), in a given state of its circuitry, can be written as Eq. 3, where the i-th element on the array is the selected element to perform the REV method. If an additional phase term ($\phi_i(\beta_i)$) is added to the field radiated by the element under test for a certain value of $\phi_i(\beta_i)$ the amplitude of $\vec{E}_{array}$ will be maximum ($\vec{E}_{max}$) or minimum ($\vec{E}_{min}$). To check for which value of ($\phi_i(\beta_i)$) total array field ($\vec{E}_{array}$) satisfies the last condition, the phase shifter of the i-th channel is swept. Knowing the phase shift value for the maximum amplitude received on the sweep and the relation between the maximum and the minimum amplitude value measured, the excitation coefficient is retrieved.

$$\vec{E}_{array} = \vec{E}_i + \sum_{\substack{n=1 \\ n\neq i}}^{N} \vec{E}_n = \vec{E}_i e^{j\phi_i(\beta_i)} + \sum_{\substack{n=1 \\ n\neq i}}^{N} \vec{E}_n \quad (3)$$

For the analyzed beamformer, performance degradation stems from amplitude fluctuations in the swept phase channel and interchannel coupling array. Moreover, static channels

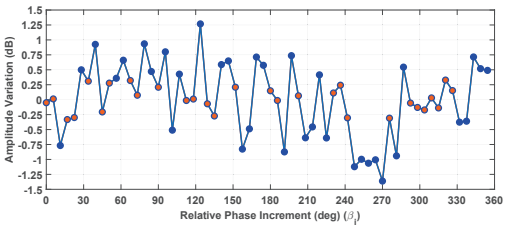

Fig. 6. Measured amplitude variation for a phase sweep with all other channels turned off. Orange dots represent those phase states with an amplitude variation within the established limits

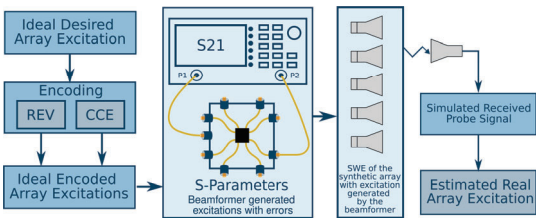

Fig. 7. Workflow of the proposed simulation method for calculating the probe received signal to simulate the calibration methods

exhibit an altered total power radiated as depicted in Fig. 3 conditioned to the phase state of the swept channel. This effect is impossible to correct due to the nature of the beamformer. For compensating the amplitude variation in the channel under test, two approaches are feasible. First, a programmable attenuator can adjust each phase state's amplitude, yet this alters coupling behavior in adjacent channels (Eq. 2). Second, selecting equispaced points close to the initial amplitude state, within a $\pm 0.35dB$ amplitude variation to perform an interpolation of the theoretical response. Fig. 6 illustrates relative gain measurements without the coupling term, where the orange dotted points represent phase states within the established boundary. Henceforth, this approach is termed *Selective-REV*.

C. Calibration based on Control Circuit Encoding

In the far-field region of a phased array with N elements, the signal received by probe b relates to the array's excitation coefficients a_i and patterns f_i (Eq. 4). When probe and array positions are fixed, $b = \sum a_i$. Since all elements radiate simultaneously, individual a_i values are unknown but can be determined from multiple measurements of b, adjusting for relative changes in a_i. This yields a linear equation system $\mathbf{b} = H\mathbf{a}$, where b represents the composite signal measured and H encodes the altered coefficients.

$$b(\theta, \phi) = \sum_{i=1}^{N} a_i f_i(\theta, \phi) \tag{4}$$

Solving this linear equations system relies on choosing a good encoding matrix H. The matrix H should have a low conditioning number and be easily invertible. Hadamard matrices satisfy all these requirements [8]. The encoding of the matrix can be performed by phase or amplitude shifting.

IV. Simulation of the Beamformer Contribution to the Encoding Errors

A simulation tool based on the spherical wave expansion of a synthetic array has been developed to model and study the impact of different error sources on the calibration procedure. The simulation of the signal received in a given point of the space is calculated by performing the spherical wave expansion of a synthetic phased array excited with coefficients provided by an S-Parameter measurement of the beamformer. This procedure allows isolating the beamformer contribution from the rest of the system under calibration, such as phased array elements defects, or mismatching in the distribution network of the array. The complete simulation workflow is shown in Fig. 7.

TABLE I
Comparison between the S-Parameter measurement and the retrieved coefficients from the different calibration methods evaluated on simulation

	S − Parameters		*REV*		*Selective − REV*		*CCE − Amplitude*		*CCE − Phase*		*CCE − Complex*	
	K(dB)	*X(°)*	*K(dB)*	*X(°)*	*K(dB)*	*X(°)*	*K(dB)*	*X(°)*	*K(dB)*	*X(°)*	*K(dB)*	*X(°)*
Beam − to − 0°												
Element#1	-0.7	-3	1.1	17	-1	2	-0.1	5	-0.1	5	-0.2	14
Element#2	1.1	13	-1.8	1	1.3	9	0.5	16	0.5	16	0.5	-88
Element#3	-0.7	3	0.1	15	0.2	5	0.0	5	0.0	5	-0.9	-53
Element#4	-0.4	10	-0.5	5	-0.4	6	-0.3	10	-0.3	10	-5.3	23
Element#5	0.4	-11	0.2	2	0.7	-6	1.0	-14	1.0	-14	-5.5	75
Element#6	-1.1	4	0.7	-13	-1.2	-2	-1.5	0	-1.5	0	-2	-12
Element#7	-0.1	-10	1.5	-30	-0.5	-5	-0.3	-19	-0.3	-19	-1.6	91
Element#8	1.4	-4	0.4	-10	-1.0	-8	0.6	-4	0.6	-4	2.9	-50
Beam − to − 20°												
Element#1	-0.8	27	-0.4	32	-0.4	31	-0.4	30	-1.1	31	-0.6	26
Element#2	0.3	-33	0.2	-26	0.5	-30	0.2	-32	-0.2	-32	-0.6	-35
Element#3	-0.9	-84	-0.2	-92	-1.2	-92	-0.6	-78	-0.5	-72	-2.2	-69
Element#4	-0.5	-138	0.3	-110	-0.1	-129	-0.7	-132	-0.3	-129	-2.6	-120
Element#5	1.0	147	0.5	160	1.3	152	0.7	152	0.5	160	-1.7	155
Element#6	0.4	90	-0.2	83	0.8	81	0.0	96	0.5	92	0.8	71
Element#7	0.1	31	0.3	23	-0.2	25	-0.1	32	0.1	30	3.1	30
Element#8	0.3	-37	-1.1	-50	-0.1	-45	0.8	35	0.7	-31	3.6	-31

Simulation results in Table 1 show an amplitude mismatch between S-Parameter measurement and the traditional REV method, mitigated by selective sample selection for the curve interpolation. Comparing CCE encoding matrices, complex encoding incurs higher errors due to channel coupling modification. Real Hadamard matrix-based phase and amplitude encodings provide a close approximation of phased array coefficients, with amplitude encoding employing a 10dB attenuation level. Selective-REV, CCE-Amplitude, and CCE-Phase encodings yield accurate results within 1dB of amplitude and ±10 degrees in phase RMS. CCE-Complex achieves an awful result due to a higher varaition of the interchannel coupling between states. Injecting these coefficients into the simulation array model of [3], Fig. 8 compares the recovered excitation coefficients for both configurations. The REV method exhibits significant amplitude imbalance, leading to erroneous side-lobe levels, while Selective-REV improves SLL level matching. The traditional REV method shows more significant phase errors. CCE patterns (Fig. 2) demonstrate similar agreement with S-Parameter measurement as Selective-REV. Broadside configuration exhibits a larger mismatch in the first right-side lobe, whereas, for the beam-steered configuration, both methods perform similarly.

V. Offline Calibration and Pattern Prediction in an Anechoic Chamber

In a complete antenna system, factors like mutual coupling between radiating elements and electromagnetic interactions with fixation elements can greatly affect calibration method performance. This includes accounting for distribution network mismatch, which remains consistent across beamformer configurations. These measurements assess whether a procedure based on passive diagram knowledge and extracted excitation coefficients can estimate the active diagram accurately without direct measurement. Fig. 1 correlates with simulated REV results, where traditional REV exhibits higher amplitude error, resulting in different side-lobe levels and asymmetry. At

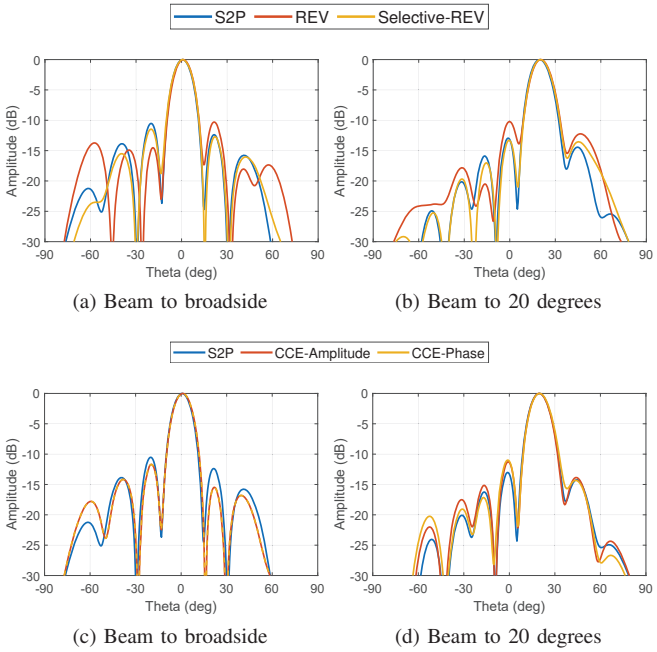

Fig. 8. Comparison of a simulated diagram using the array coefficients measured in S-Parameters and the simulated calibration methods

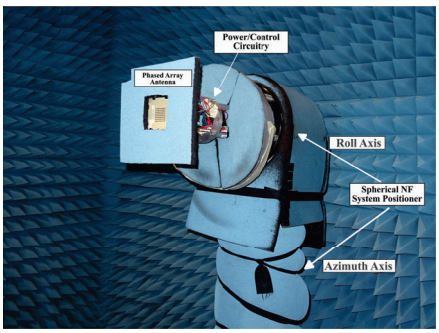

Fig. 9. Measurement setup for 64 elements active phased array on the LEHA SNF facility

20-degree beam steering, a 3-degree aiming mismatch exists between traditional REV and Selective-REV. The Selective-REV method yields a pattern closer to real measurement, with more accurate SLL imbalance and level, especially in steered beam configuration. Beam direction aligns within uncertainty compared to active pattern measurement. CCE encoding demonstrates good agreement with measured encodings and active patterns, consistent with simulations. The comparative error between Selective-REV and CCE encodings falls within measurement uncertainty, making it challenging to determine the more accurate result compared to real measurement.

VI. Conclusions

This article delves into the non-idealities of commercial beamformers and their impact on phased array antenna calibration. Extensive S-Parameter measurements were conducted to understand these effects on excitation retrieval techniques. Peripheral probe calibration methods were adjusted for highly integrated phased-array antennas, revealing errors introduced by non-idealities during excitation decoding. An adapted REV method aimed to reduce retrieval errors in active phased arrays. Complex Hadamard matrices were explored but

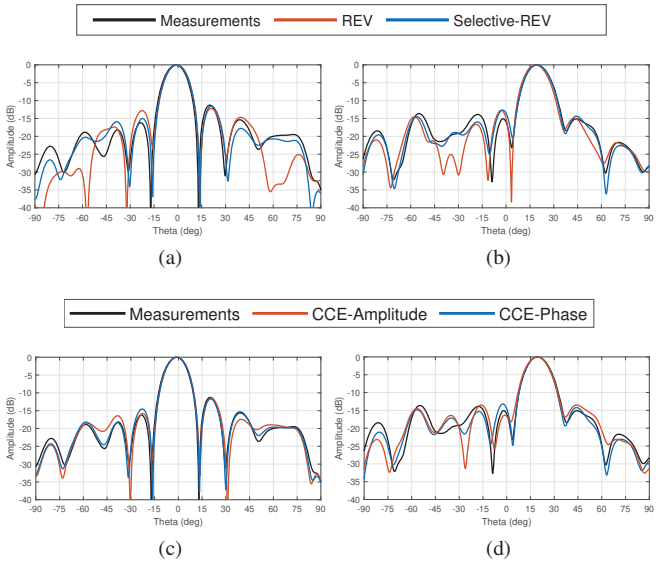

Fig. 10. Comaprison between the measured diagram and the predicted using the proposed calibration methods

showed limited performance due to beamformer constraints. Synthetic array models compared pattern predictions to real beamformer-generated patterns, revealing accurate estimations with CCE encoding using real Hadamard matrices and the Selective-REV method. Both calibration methods were performed in an anechoic chamber achieving an agreement between predicted and measured patterns, showcasing Selective-REV's efficacy in reducing excitation coefficient retrival errors. These methods are suitable for accurate pattern prediction, as demonstrated by the correlation between synthetic and active measurements.

References

[1] 3GPP TS 38.101-2 5G; NR; *User Equipment (UE) radio transmission and reception; Part 2: Range 2 Standalone* v15.3.0, Sep. 2018.

[2] K. Kibaroglu, M. Sayginer, T. Phelps and G. M. Rebeiz, "A 64-Element 28-GHz Phased-Array Transceiver With 52-dBm EIRP and 8–12-Gb/s 5G Link at 300 Meters Without Any Calibration," in *IEEE Transactions on Microwave Theory and Techniques*, vol. 66, no. 12, pp. 5796-5811, Dec. 2018.

[3] A. T. Muriel-Barrado, J. Calatayud-Maeso, A. Rodríguez-Gallego, P. Sánchez-Olivares, J. M. Fernández-González and M. Sierra-Pérez, "Evaluation of a Planar Reconfigurable Phased Array Antenna Driven by a Multi-Channel Beamforming Module at Ka Band," in *IEEE Access*, vol. 9, pp. 63752-63766, 2021.

[4] T. Yu and G. M. Rebeiz, "A 22–24 GHz 4-Element CMOS Phased Array With On-Chip Coupling Characterization," in *IEEE Journal of Solid-State Circuits*, vol. 43, no. 9, pp. 2134-2143, Sept. 2008.

[5] K. K. Wei Low, A. Nafe, S. Zihir, T. Kanar and G. M. Rebeiz, "A Scalable Circularly-Polarized 256-Element Ka-Band Phased-Array SATCOM Transmitter with ±60° Beam Scanning and 34.5 dBW EIRP". Presented at *IEEE MTT-S International Microwave Symposium (IMS)*, Boston, MA, USA, 2019, pp. 1064-1067.

[6] S. Mano and T. Katagi, "A method for measuring the amplitude and phase of each radiating element of a phased array antenna," *Electronics and Communications in Japan (Part I: Communications)*, vol. 65, no. 5, pp. 58–64, 1982.

[7] E. Lier, M. Zemlyansky, D. Purdy and D. Farina, "Phased array calibration and characterization based on orthogonal coding: Theory and experimental validation". Presented at *IEEE International Symposium on Phased Array Systems and Technology*, Waltham, MA, USA, 2010, pp. 271-278.

[8] Tadej, Wojciech & Zyczkowski, Karol. (2006). "A Concise Guide to Complex Hadamard Matrices" in *Open Systems & Information Dynamics*, vol 13, pp. 133-177.